Fermi resonance in dynamical tunneling in a chaotic billiard

Chang-Hwan Yi,[1,*] Ji-Hwan Kim,[2] Hyeon-Hye Yu,[2] Ji-Won Lee,[1] and Chil-Min Kim[1,†]
[1]*Department of Emerging Materials Science, DGIST. Hyeonpung-myeon Dalseong-gun, Daegu 711-873, Korea*
[2]*Department of Physics, Sogang University, Seoul, 121-742, Korea*
(Received 19 August 2014; revised manuscript received 22 April 2015; published 20 August 2015)

We elucidate that Fermi resonance ever plays a decisive role in dynamical tunneling in a chaotic billiard. Interacting with each other through an avoided crossing, a pair of eigenfunctions are coupled through tunneling channels for dynamical tunneling. In this case, the tunneling channels are an islands chain and its pair unstable periodic orbit, which equals the quantum number difference of the eigenfunctions. This phenomenon of dynamical tunneling is confirmed in a quadrupole billiard in relation with Fermi resonance.

DOI: 10.1103/PhysRevE.92.022916 PACS number(s): 05.45.Mt, 42.55.Sa, 42.55.Px

I. INTRODUCTION

Dynamical tunneling, which is a subset of quantum phenomenon in a chaotic system, was suggested by Davis and Heller in 1981 by considering the analogy of the barrier tunneling phenomena in the one-dimensional symmetric double well [1,2]. In this phenomenon, two eigenstates, which are localized on classically disconnected regions in phase space, can be quantum-mechanically coupled with each other. Since the report, the phenomenon has been intensively studied and found in various chaotic systems such as molecules [3], billiards [4–6], microcavities [7–10], cold atom systems [11,12], and a nanowire [13]. Through the studies, several variations have been theoretically and experimentally found [2–17].

Among the variations, chaos-assisted tunneling [4,5,11,12] and resonance-assisted tunneling [2,14,16] are much studied. In the case of chaos-assisted tunneling, the chaotic dynamics of the corresponding generic classical Hamiltonian system can quantum-mechanically mediate dynamical tunneling between two regular regimes in classical phase space even though the probabilities of the direct dynamical tunneling are very small for the distance between the two regular regimes is too far. In the case of resonance-assisted tunneling, a pair of eigenfunctions localized on classically disconnected regions are quantum-mechanically coupled through classical resonances. When two eigenfunctions are coupled with each other, the pair of coupled eigenfunctions due to dynamical tunneling do not seem to be supported by a pair of periodic orbits because, according to a report [3], they are either irregular or scarred by other periodic orbits. Hence, the coupled eigenfunctions seemingly not satisfying the Fermi resonance relation and dynamical tunneling has been regarded as a different phenomenon from scar formation. Recently, it was proved that scar formation is the phenomenon of Fermi resonance [18].

In this manuscript, however, we elucidate for the first time that dynamical tunneling is the phenomenon of Fermi resonance in a chaotic billiard. In this two-dimensional system, when an eigenfunction localized on a periodic orbit interacts with another eigenfunction, coupled eigenfunctions caused by dynamical tunneling are also the superposed states of a pair of eigenfunctions and the tunneling channels are supported by a pair of periodic orbits, which are governed by the Poincaré-Birkhoff theorem (PBT) [19]. Hence the periodic orbits of the tunneling channels equals the quantum number difference of the original normal modes of the eigenfunctions.

To prove this phenomenon, this paper is organized as follows: in Sec. II, we show the relation between dynamical tunneling and Fermi resonance in a two-dimensional quadrupole billiard; in Sec. III, we demonstrate Fermi resonance in dynamical tunneling when an eigenfunction localized on a periodic orbit interact with another eigenfunction in this billiard; in Sec. IV, we discuss the phenomenon of Fermi resonance in dynamical tunneling and conclude our results.

II. DYNAMICAL TUNNELING IN A QUADRUPOLE BILLIARD

The role of Fermi resonance in dynamical tunneling is examined in a quadrupole billiard, which is given as follows:

$$r(\theta) = R(1 + \varepsilon \sin 2\theta), \tag{1}$$

where ε is the deformation parameter, R is the radius of the circle at $\varepsilon = 0$, and θ is the angle from the x axis in polar coordinate. We obtain eigenvalues depending on ε by solving the Helmholtz equation by the boundary element method with the Dirichlet boundary condition [20,21]. In obtaining eigenvalues, the cavity area is preserved as ε increases.

A. Eigenvalue spectrum and interactions

Figure 1 is the eigenvalues in the region $\varepsilon < 0.1$ and $21 < kR < 24$, where k is the vacuum wave number. In the figure, the $(l,m) = (1,18)$ and the $(2,14)$ normal mode, which are eigenfunctions in a circular billiard, interact with each other around A. Here l and m are the radial and the angular quantum number in polar coordinate, respectively. Due to the interaction, a pair of eigenfunctions are generated, which are localized on a diamond-shaped periodic orbit and on its pair rectangular-shaped unstable periodic orbit, respectively. The diamond-shaped and the rectangular-shaped periodic orbit is a pair of periodic orbits in the sense of the PBT. Hereafter, in order to avoid confusion, when no specific concern is given, the pair of periodic orbits referred to in this paper imply an elliptic and a hyperbolic fixed points following the PBT, which are a pair. In this interaction, an avoided

*yichanghwan@hanmail.net
†chmkim@dgist.ac.kr

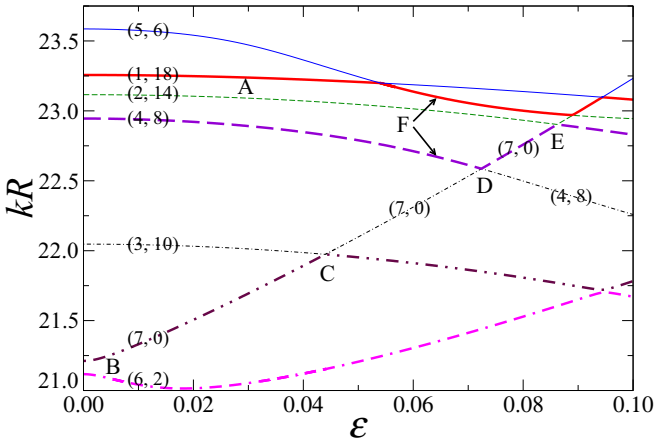

FIG. 1. (Color online) Eigenvalue spectrum in a quadrupole billiard depending on the deformation parameter. Around A, a pair of normal modes labeled by (1,18) and (2,14) interact with each other through an AC and a pair of eigenfunctions are generated, which are localized on a diamond-shaped periodic orbit and on its pair rectangular-shaped unstable periodic orbit, respectively. Around B, the (6,2) and the (7,0) normal mode interact with each other and a pair of bouncing-ball type modes (BBTMs) are generated: one is vertical and the other horizontal. Around C, a vertical BBTM, generated from the (7,0) normal mode, and a (3,10) normal mode interact with each other. Around D, a vertical and a horizontal BBTM interact with each other through an AC for dynamical tunneling. Around E, a rectangular scar interacts with a vertical BBTM. We mainly focus on ACs around C and D in this paper to elucidate the phenomenon of dynamical tunneling.

crossing (AC) takes place over a broad range, which is the typical Demkov-type interaction [22]. Around B, the (7,0) and the (6,2) normal mode generate a pair of bouncing-ball-type modes (BBTMs): one is vertical and the other horizontal. The vertical BBTM is localized on a period-2 periodic orbit and the horizontal one on its pair period-2 unstable periodic orbit. On further increase of ε, the vertical BBTM interacts with the (3,10) normal mode around C. After the interaction, the original eigenfunctions are recovered by exchanging their properties. This is the typical Landau-Zener-type interaction [23,24], which takes place in a narrow range. On further increase of ε, the vertical BBTM interacts with the horizontal BBTM developed from the (4,8) normal mode around D. The horizontal BBTM is caused by the interaction of the (4,8) normal mode with a horizontal BBTM developed from the (5,6) normal mode around F. The AC around F is also the Demkov-type interaction. After the interaction around D, the original eigenfunctions are also recovered by exchanging their properties. Around E, the vertical BBTM interacts with the scar localized on a rectangular unstable periodic orbit. After the interaction, the original eigenfunctions are also recovered by exchanging their properties due to the Landau-Zener-type interaction.

B. Fermi resonance in dynamical tunneling

For the Landau-Zener-type interaction around D in Fig. 1, we can see that the two eigenfunctions are nearly degenerated. Then the Hamiltonians of the two eigenfunctions can be described by $H(I_1,I_2)$ and $H(I_1',I_2')$, where I_i and I_i' are the action variables and the subscripts 1 and 2 are the degrees of freedom. When $|I_i' - I_i| \ll 1$, we can obtain the following condition by expanding $H(I_1',I_2')$ around $H(I_1,I_2)$:

$$(I_1 - I_1')\omega_1 + (I_2 - I_2')\omega_2 = 0, \tag{2}$$

where $\omega_i = \partial H/\partial I_i$ is the frequency associated with the action I_i. Since $I_i = (n_i + \alpha_i/4)$, we can obtain the relation $|n_1 - n_1'|\omega_1 = |n_2 - n_2'|\omega_2$ for two eigenstates (n_1,n_2) and (n_1',n_2'), where α_i is the Maslov index. According to Berry and Tabor, when winding number ω_1/ω_2 is rational, the orbit is periodic [25]. Then we can obtain the following relation for Fermi resonance by letting that $\omega_1 = m_1$ and $\omega_2 = m_2$:

$$(|\Delta n_1|,|\Delta n_2|) = (m_2,m_1), \tag{3}$$

where (m_2,m_1) is the classical periodic orbit, which should be determined according to the cavity morphology [18], and $(|\Delta n_1|,|\Delta n_2|)$ is the quantum number difference of two quantum states (n_1,n_2) and (n_1',n_2') such that $|\Delta n_1| = |n_1 - n_1'|$ and $|\Delta n_2| = |n_2 - n_2'|$. In a quadrupole cavity, m_1 and m_2 are the number of bounces on each degree of freedom of a periodic orbit. Because the quantum number difference $(|\Delta n_1|,|\Delta n_2|)$ implies a pair of superposed states, the periodic orbit (m_2,m_1) should support the superposed states. This is the phenomenon of Fermi resonance. According to the PBT, the periodic orbit (m_2,m_1) implies the stable and the unstable periodic orbit, which are a pair. When the vertical BBTM developed from (7,0) normal mode interacts with the horizontal one developed from the (4,8) normal mode, coupled states should be localized on the (3,8) periodic orbits. This is the very dynamical tunneling.

III. DYNAMICAL TUNNELING THROUGH PERIODIC ORBITS

To understand the phenomenon of dynamical tunneling, we obtain the intensity plots of eigenfunctions around D as shown in Fig. 2. Figures 2(a) and 2(b) are the vertical and the horizontal BBTM at $\varepsilon = 0.0723$, which are developed from the (7,0) and the (4,8) normal mode, respectively. When the two BBTMs interact with each other through an AC, the two eigenfunctions are coupled as shown in Figs. 2(c) and 2(d) at $\varepsilon = 0.0724$. In order to show that these states are quantum-mechanically superposed states, the two BBTMs shown in Figs. 2(a) and 2(b) are superposed. As are shown in Figs. 2(e) and 2(f), $[(7,0) + (4,8)]/\sqrt{2}$ and $[(7,0) - (4,8)]/\sqrt{2}$ states are the same as the eigenfunctions shown in Figs. 2(c) and 2(d), respectively. We note here that (7,0) and (4,8) denote the vertical and the horizontal BBTM developed from the (7,0) and the (4,8) normal mode, respectively. This result is an evidence of Fermi resonance. After the AC, the BBTMs are recovered by exchanging their properties. The coupled states, as they are the phenomenon of Fermi resonance, should satisfy the Fermi resonance relation $(|\Delta l|,|\Delta m|) = (p_\theta, p_r) = (3,8)$, where p_θ is the number of librations on the angular axis and p_r is the number of bounces on the boundary. At a glance, the patterns shown in Figs. 2(c) and 2(d) do not seem to be

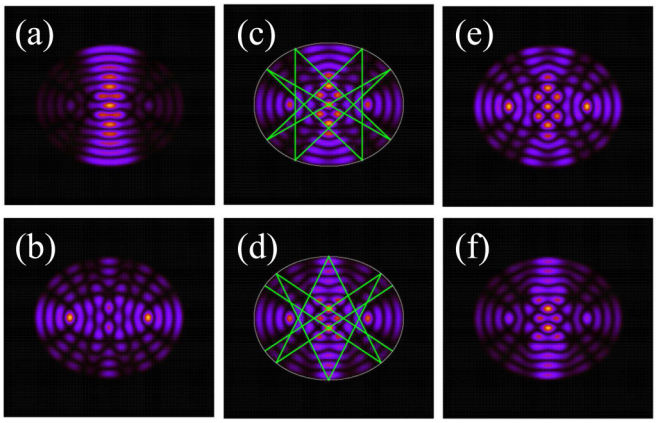

FIG. 2. (Color online) Intensity plots of eigenfunctions around D. (a), (b) The vertical and the horizontal BBTM, respectively, at $\varepsilon = 0.0723$. (c), (d) A pair of coupled states when the vertical and the horizontal BBTM interact with each other at $\varepsilon = 0.0724$. (e), (f) The symmetric and antisymmetric superposition of the wave functions of (a) and (b) at $\varepsilon = 0.0723$, respectively. The trajectories shown in (c) and (d) are a stable and an unstable $(m_\theta, m_r) = (3,8)$ periodic orbit, which are a pair in the sense of the PBT. The color order from the maximum to the minimum value is yellow, purple, and black.

supported by the (3,8) periodic orbits, which are superimposed on the intensity plot of the eigenfunctions.

In order to elucidate the role of Fermi resonance in dynamical tunneling, Husimi functions are obtained. Figures 3(a) and 3(b) are the Husimi functions of the vertical and the horizontal BBTM superimposed on classical trajectories in phase space, respectively. The two BBTMs are localized on a period-2 stable periodic orbit and a period-2 unstable

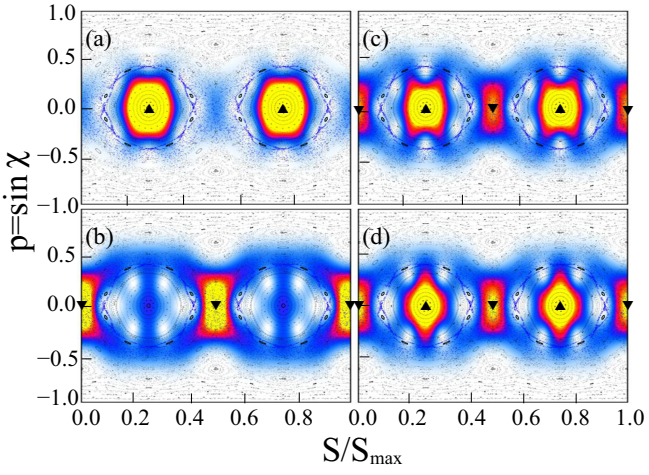

FIG. 3. (Color online) Husimi functions superimposed on classical trajectories. (a), (b) The Husimi functions of the vertical and the horizontal BBTM, respectively. (c), (d) The Husimi functions of the coupled states shown in Figs. 2(c) and 2(d), respectively. The classical trajectories exhibit a period-8 stable (upward triangles) and an unstable periodic orbit (downward triangles) comprising a period-8 islands chain. χ is the incident angle, S is the arc length from the x axis, and $S_{\max}$ is the boundary length. The color order from the maximum to the minimum value is yellow, red, blue, and white.

periodic orbit, respectively, as shown by the yellow bright spots around triangles (upward for stable and downward for unstable). The vertical BBTM, as it is caused by the interaction of the (7,0) normal mode with the (6,2) one, should be localized on the (1,2) periodic orbit. Similarly, the horizontal BBTM, as it is caused by the interaction of the (4,8) normal mode with the (5,6) horizontal BBTM around F, should be localized on the (1,2) unstable periodic orbit. Hence the vertical and the horizontal BBTM satisfy the Fermi resonance relation $(|\Delta l|, |\Delta m|) = (p_\theta, p_r) = (1,2)$. This is the very Fermi resonance in formation of scars [18,26–28]

When an AC takes place, the two BBTMs are coupled as shown by the Husimi functions in Figs. 3(c) and 3(d). In both figures, the yellow bright spots are placed on a period-2 stable periodic orbit and a period-2 unstable periodic orbit and wave functions are connected with each other as shown by the weak blue distributions between the two regions. This connection is classically forbidden because the stable and the unstable periodic orbit are disconnected by the secondary islands chain and Kolmogorov-Arnold-Moser (KAM) barriers in phase space. Such distributions are made possible only by dynamical tunneling. This result may not seem to satisfy the Fermi resonance relation because while the quantum number difference of the two BBTMs is (3,8), the yellow bright spots are neither localized on the (3,8) stable periodic orbit nor on the (3,8) unstable periodic orbit. However, with much attention, we can see faint channels connecting the two BBTMs. The tunneling channels in Fig. 3(c) are localized on a period-8 stable periodic orbit, while those in Fig. 3(d) are localized on a period-8 unstable periodic orbit. The stable and the unstable periodic orbit of the period-8 islands chain are the tunneling channels for dynamical tunneling.

In order to clearly show the tunneling channels, the log-plot of the Husimi functions superimposed on classical trajectories are obtained as shown in Fig. 4. Figure 4(a) clearly exhibits 16 tunneling channels on two period-8 stable orbits. The 16 tunneling channels are caused by two opposite traveling directions of the (3,8) periodic orbit. The figure also shows 16 zeros of Husimi function [28] around two period-8 unstable periodic orbits, which appear as local-minimum regions. Because an eigenfunction is not distributed on the zeros of the Husimi function, dynamical tunneling takes place through the stable periodic orbits of the islands chains, which is classically forbidden. In contrast to those of the stable periodic orbits, the tunneling channels in Fig. 4(b) are two period-8 unstable periodic orbits. Here, we can discern 12 zeros of Husimi function. The large size zeros of Husimi function around $p = 0$ are caused by two close zeros of Husimi function not by a single one. This result verifies that when the two BBTMs developed from the (7,0) and the (4,8) normal mode interact with each other, the quantum number difference $(|\Delta l|, |\Delta m|) = (3,8)$ equals the $(p_\theta, p_r) = (3,8)$ periodic orbit, where the tunneling channels are localized. Hence dynamical tunneling also satisfies the Fermi resonance relation.

For a more quantitative justification of the tunneling channels, we transform the trajectories on (s, p) coordinate into polar coordinate. First, the s coordinate is transformed into $\xi = 4s/s_{\max} - 1$ as shown in Fig. 5(a). Then, the trajectories on the left half coordinate can be transformed into polar

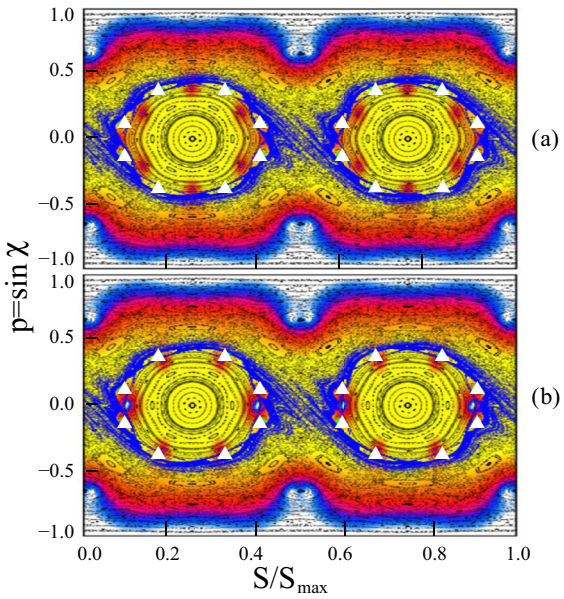

FIG. 4. (Color online) Log plot of the Husimi function superimposed on classical trajectories. (a), (b) The Husimi functions of the eigenfunctions shown in Figs. 2(c) and 2(d), respectively. Elliptically distributed local-minimum points around the islands chains are the zeros of the Husimi function. χ is the incident angle, S is the arc length from the x axis, and $S_{\max}$ is the boundary length. Triangles are stable fixed points of a (4,8) islands chain. The color order from the maximum to the minimum value is yellow, red, blue, and white.

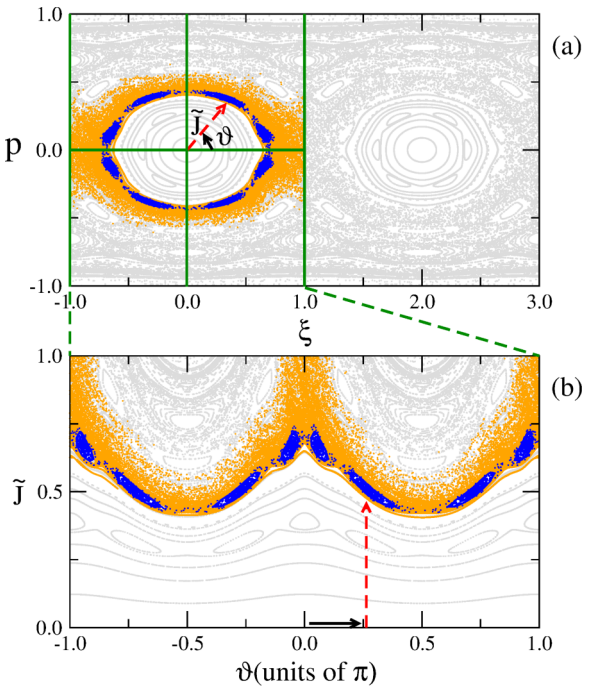

FIG. 5. (Color online) Trajectories on Birkhoff coordinate and on polar coordinate when the deformation parameter is $\varepsilon = 0.0724$. (a) The trajectories on Birkhoff coordinate, and (b) is those on polar coordinate. The horizontal and the vertical axis are defined by Eqs. (4) and (5), respectively.

coordinate as follows:

$$\vartheta = \arctan\left(\frac{p}{\xi}\right), \tag{4}$$

$$\tilde{J} = \sqrt{p^2 + \xi^2}, \tag{5}$$

where $\tilde{J}$ is the distance from the center to the trajectory and ϑ is the angle as shown in Fig. 5(a). To note here, we apply the transformation to only the half plane of the original phase space since it has a virtue of symmetry. The trajectories transformed into polar coordinate are shown in Fig. 5(b). For example, the arrow shown in Fig. 5(a) is transformed as indicated in Fig. 5(b).

By using the same mechanism of the transformation, we obtain the transformed Husimi functions on polar coordinate as shown in Fig. 6. Figures 6(a) and 6(b) are the vertical and the horizontal BBTM on polar coordinate at $\varepsilon = 0.0714$. When they interact with each other, the transformed Husimi functions also exhibit zeros of Husimi functions as shown in Figs. 6(c) and 6(d), around $\tilde{J} = 0.5$, which are the $[(7,0) + (4,8)]/\sqrt{2}$ and the $[(7,0) - (4,8)]/\sqrt{2}$ state at $\varepsilon = 0.0724$, respectively.

In order to obtain the intensity variation of the Husimi functions around the tunneling channel depending on the deformation parameter, we obtain adiabatic KAM curves [29,30], which correspond to the period-8 islands chain. The adiabatic KAM curves in Birkhoff-coordinate are given as follows:

$$p(s) = \sin\chi(s) = \sqrt{1 - (1 - \tilde{p}^2)\kappa(s)^{2/3}}, \tag{6}$$

where $\tilde{p}$ is the parameter determining the curves and κ is the curvature of the system boundary depending on the s. For the curves to cross the stable points of the period-8 islands chain, we set $\tilde{p} = 0.270$ for $\varepsilon = 0.0714$ and $\tilde{p} = 0.275$ for $\varepsilon = 0.0724$. In these parameters, the adiabatic KAM curves pass through the center of the islands chain. The curves are also transformed into polar coordinate, that is, $\gamma(s,p;\tilde{p})$ to $\gamma(\vartheta,\tilde{J})$. The curves are plotted in Fig. 6 as thin "w"-like lines. In Figs. 6(c) and 6(d), we also plot highlighted period-8 islands chains. It is stressed that the adiabatic KAM curves and the islands chains well coincide.

Now, we obtain the intensity of the Husimi functions along the adiabatic KAM curves depending on the deformation parameter as shown in Fig. 7. As is shown in Fig. 7(a), when there is no tunneling, the intensities of the Husimi functions of the vertical and the horizontal BBTM are almost uniform along the adiabatic KAM curves as shown by the thin dashed blue and the thin solid red curve. Obviously, when dynamical tunneling takes place, the intensity around the islands chain is much higher than that around the unstable periodic orbit as shown by the thick dashed (blue) curve as shown in Fig. 7(a), which is the $[(7,0) + (4,8)]/\sqrt{2}$ state. In contrast to the thick dashed (blue) curve, in the case of the $[(7,0) - (4,8)]/\sqrt{2}$ state, the intensity around the unstable periodic orbit is much higher than that around the islands chain as shown by the thick solid (red) curve in Fig. 7(a). Figure 7(b) shows the position of the islands chain and the unstable periodic orbits. This analysis quantitatively elucidates the tunneling channels when dynamical tunneling takes place.

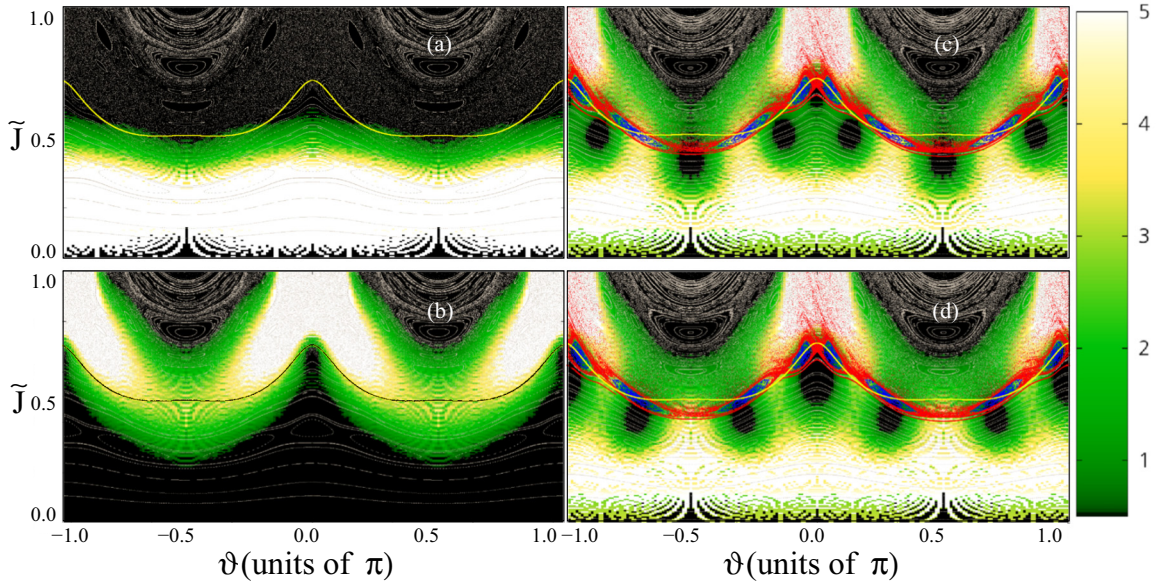

FIG. 6. (Color online) Husimi functions $h(\vartheta,\tilde{J})$ superimposed on classical trajectories on polar coordinate. (a), (b) The Husimi functions of the vertical and the horizontal BBTM at $\varepsilon = 0.0714$, respectively. (c), (d) The Husimi functions of Figs. 2(c) and 2(d) at $\varepsilon = 0.0724$, respectively, when an AC takes place. Thin "w"-like lines (yellow in (a), (c), and (d) and black in (b)) in the figures are the adiabatic KAM curves γ. (a), (b) When $\tilde{p} = 0.270$; (c), (d) when $\tilde{p} = 0.275$. The horizontal and the vertical axes are defined by Eqs. (4) and (5), respectively. The color order from the maximum to the minimum value is white, green, and black.

The tunneling channels satisfying the Fermi resonance relation are easily observed when an eigenfunction localized on a periodic orbit interacts with the other eigenfunctions. As another example, we take an interaction around C, where the (3,10) normal mode interacts with the vertical BBTM developed from the (7,0) normal mode. Figures 8(a) and 8(b) are the normal mode and the vertical BBTM at $\varepsilon = 0.043\,00$, respectively. When the two eigenfunctions interact with each other, they exhibit a pair of coupled states as shown in Figs. 8(c) and 8(d) at $\varepsilon = 0.043\,99$, respectively. These states are also quantum-mechanically superposed states. The trajectories on the figures are the (4,10) periodic orbits. Figures 8(e) and 8(f) are the eigenfunctions of the vertical BBTM and the normal mode at $\varepsilon = 0.045\,00$, which are recovered after an AC, respectively. The coupled states, as they are the phenomenon of Fermi resonance, should also satisfy the Fermi resonance relation $(|\Delta l|,|\Delta m|) = (p_\theta, p_r) = (4,10)$. The eigenfunctions shown in Figs. 8(c) and 8(d) do not also seem to be supported by the (4,10) periodic orbits, which are superimposed on the intensity plot of the coupled states.

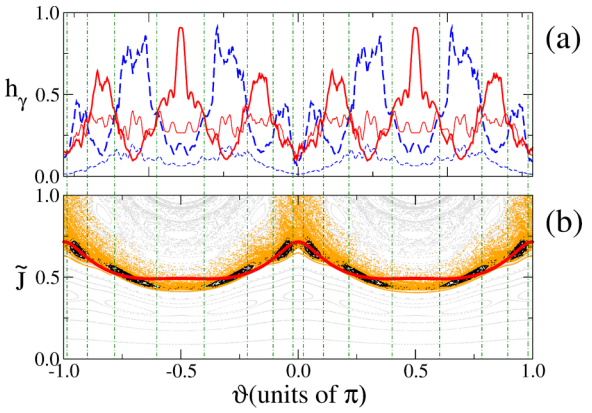

FIG. 7. (Color online) Intensities of Husimi functions along the adiabatic KAM curves γ. (a) The intensity of each Husimi function along the adiabatic KAM curves γ in Fig. 6. Solid (red) thin and thick lines correspond to Figs. 6(a) and 6(c), respectively. Dashed (blue) thin and thick lines correspond to Figs. 6(b) and 6(d), respectively. (b) The classical trajectories and the adiabatic KAM curve γ on polar coordinate at $\varepsilon = 0.0724$. Vertical (green) dot dashed lines show the region of the islands chain.

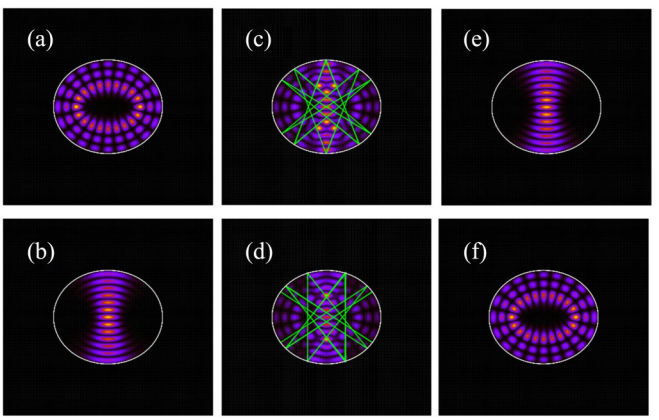

FIG. 8. (Color online) Eigenfunctions around C in Fig. 1. (a), (b) The (3,10) normal mode and the vertical BBTM developed from the (7,0) normal mode at $\varepsilon = 0.043\,00$, respectively. (c), (d) The coupled eigenfunctions at the AC point, $\varepsilon = 0.043\,99$. (e), (f) The recovered BBTM and (3,10) normal mode after the AC at $\varepsilon = 0.045\,00$, respectively. The color order from the maximum to the minimum value is yellow, purple, and black.

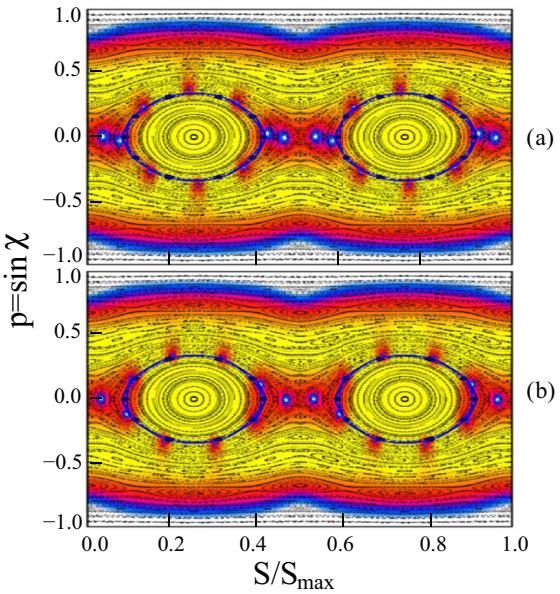

FIG. 9. (Color online) Log plot of the Husimi function superimposed on classical trajectories. (a), (b) The Husimi functions of the eigenfunction shown in Figs. 8(c) and 8(d) at $\varepsilon = 0.043\,99$, respectively. Elliptically distributed local-minimal points around the islands chains are the zeros of the Husimi function. The color order from the maximum to the minimum value is yellow, red, blue, and white.

Figures 9(a) and 9(b) are the log-plots of the Husimi functions of the eigenfunctions shown in Figs. 8(c) and 8(d), respectively. Figures 9(a) and 9(b) clearly exhibit 20 tunneling channels on two period-10 stable and on two period-10 unstable periodic orbits, respectively. The 20 tunneling channels are caused by two opposite traveling directions of the (4,10) periodic orbit. Figures 9(a) and 9(b) also show 20 zeros of Husimi function around two period-10 unstable periodic orbits and two period-10 stable periodic orbits, respectively. This result also verifies that when the two eigenfunctions developed from the (7,0) and the (3,10) normal mode interact with each other, the quantum number difference $(|\Delta l|,|\Delta m|) = (4,10)$ equals the $(p_\theta, p_r) = (4,10)$ periodic orbit, where the tunneling channels are localized.

Similarly, when the horizontal BBTM developed from the (6,8) normal mode interacts with the (3,16) normal mode, dynamical tunneling takes place. In this case, the (3,8) quantum number difference of the pair also equals the (3,8) periodic orbit of the tunneling channels. Hence we can say that when an eigenfunction localized on a periodic orbit interacts with another eigenfunction through an AC in a narrow range, a pair of quantum-mechanically coupled states are generated at the AC point due to dynamical tunneling. Here, the orbit of the tunneling channels equals the quantum number difference of each pair such that $(|\Delta l|,|\Delta m|) = (p_\theta, p_r)$, which is the Fermi resonance relation.

IV. DISCUSSIONS AND CONCLUSION

It is generally known that dynamical tunneling is a phenomenon distinctive from scar formation. For example, in the latter, a scar is localized on an unstable periodic orbit due to Fermi resonance [18,26], but in the former, a coupled state seems to be either irregular or scarred by other periodic orbits not satisfying the Fermi resonance relation. And while scars are generated by an interaction of a pair of normal modes [18,26], dynamical tunneling takes place when an eigenfunction localized on a periodic orbit interacts with another eigenfunction. Here, the quantum numbers of the eigenfunctions cannot be defined in a chaotic billiard. However, through our investigation, we elucidate that dynamical tunneling and scar formation are the same phenomenon of Fermi resonance. First, in both cases, a pair of eigenfunctions are the quantum-mechanically superposed states of a pair of original eigenfunctions and, second, they satisfy the Fermi resonance relation. According to a report [3], when an AC takes place in a narrow range of a deformation parameter, original wave functions are recovered by exchanging their properties after the AC, and when it takes place over a broader range, scars keep their eigenfunctions. The former is dynamical tunneling due to the Landau-Zener-type interaction [23,24] and the latter scar formation is due to the Demkov type [22].

In Ref. [17], quantum manifestation of the PBT is analyzed in the Harper map. In this map, when two eigenfunctions interact with each other through an AC, two coupled eigenfunctions are localized on a stable and on an unstable periodic orbit, respectively. After the interaction their original eigenfunctions are recovered by exchanging their properties. During the interaction, the quantum number difference equals the period of the periodic orbits, which is a phenomenon of dynamical tunneling. In a chaotic billiard, in general, when dynamical tunneling takes place, two coupled eigenfunctions are not localized on periodic orbits, but tunneling channels are localized on the periodic orbits. Detailed discussions on this phenomenon will appear elsewhere later.

In conclusion, we have investigated dynamical tunneling in a quadrupole billiard. When an eigenfunction localized on a periodic orbit interacts with another eigenfunction, the two eigenfunctions are coupled through dynamical tunneling. In this case, because a pair of periodic orbits are the tunneling channels for dynamical tunneling, the quantum number difference of two eigenfunctions equals the periodic orbits such that $(|\Delta l|,|\Delta m|) = (p_\theta, p_r)$. Hence a pair of eigenfunctions tunnel through the periodic orbits. This is the Fermi resonance relation. These results imply that Fermi resonance plays a decisive role when two eigenfunctions interact with each other through an AC. Our results will promote a deeper understanding of dynamical tunneling and provide a fundamental knowledge for analyzing complex eigenfunctions, which appear not only in physical, chemical, and optical systems but also in engineering systems.

ACKNOWLEDGMENTS

This research was supported by Basic Science Research Program (Grant No. NRF-2013R1A1A2060846) and High-Tech Convergence Technology Development Program (Grant No. NRF-2014M3C1A3051331) through the National Research Foundation of Korea (NRF) funded by the Ministry of Science, ICT & Future Planning.

[1] M. J. Davis and E. J. Heller, J. Chem. Phys. **75**, 246 (1981).
[2] O. Bohigas, S. Tomsovic, and D. Ullmo, Phys. Rep. **223**, 43 (1993).
[3] F. Z. Arranz, F. Borondo, and R. M. Benito, J. Chem. Phys. **107**, 2395 (1997).
[4] E. Doron and S. D. Frischat, Phys. Rev. Lett **75**, 3661 (1995).
[5] C. Dembowski, H.-D. Gräf, A. Heine, R. Hofferbert, H. Rehfeld, and A. Richter, Phys. Rev. Lett. **84**, 867 (2000).
[6] A. Bäcker, R. Ketzmerick, S. Löck, M. Robnik, G. Vidmar, R. Höhmann, U. Kuhl, and H.-J. Stöckmann, Phys. Rev. Lett. **100**, 174103 (2008).
[7] G. Hackenbroich and J. U. Nöckel, Europhys. Lett. **39**, 371 (1997).
[8] S. Shinohara, T. Harayama, T. Fukushima, M. Hentschel, T. Sasaki, and E. E. Narimanov, Phys. Rev. Lett. **104**, 163902 (2010).
[9] J. Yang, S.-B. Lee, S. Moon, S.-Y. Lee, S. W. Kim, Truong Thi Anh Dao, J.-H. Lee, and K. An, Phys. Rev. Lett. **104**, 243601 (2010).
[10] M.-W. Kim, S. Rim, C.-H. Yi, and C.-M. Kim, Opt. Express **21**, 32508 (2013).
[11] D. A. Steck, W. H. Oskay, and M. G. Raizen, Science **293**, 274 (2001).
[12] W. K. Hensinger *et al.*, Nature **412**, 52 (2001).
[13] J. Feist, A. Bäcker, R. Ketzmerick, S. Rotter, B. Huckestein, and J. Burgdörfer, Phys. Rev. Lett. **97**, 116804 (2006).
[14] O. Brodier, P. Schlagheck, and D. Ullmo, Phys. Rev. Lett. **87**, 064101 (2001).
[15] A. Shudo and K. S. Ikeda, Phys. Rev. Lett. **74**, 682 (1995).
[16] S. Löck, A. Bäcker, R. Ketzmerick, and P. Schlagheck, Phys. Rev. Lett. **104**, 114101 (2010).
[17] D. A. Wisniacki, M. Saraceno, F. J. Arranz, R. M. Benito, and F. Borondo, Phys. Rev. E **84**, 026206 (2011).
[18] C. H. Yi, H. H. Yu, J. W. Lee, and C. M. Kim, Phys. Rev. E **91**, 042903 (2015).
[19] A. J. Lichtenberg and M. A. Lieberman, *Regular and Chaotic Dynamics*, 2nd ed. (Springer-Verlag, New York, 1992).
[20] M. V. Berry, F. R. S., and M. Wilkinson, Proc. R. Soc. Lond. A **392**, 15 (1984).
[21] A. Bäker and R. Schbert, J. Phys. A: Math. Gen. **35**, 538 (2002).
[22] Y. N. Demkov and V. I. Osherov, Sov. Phsy. JETP **26**, 916 (1968).
[23] L. D. Landau, Phys. Z. Sowjetunion **2**, 46 (1932).
[24] C. Zener, Proc. R. Soc. Lond. A **137**, 696 (1932).
[25] M. V. Berry and M. Tabor, Proc. Roy. Soc. London A **349**, 101 (1976).
[26] F. J. Arranz, F. Borondo, and R. M. Benito, Phys. Rev. Lett. **80**, 944 (1998).
[27] F. J. Arranz, L. Seidel, C. G. Giralda, R. M. Benito, and F. Borondo, Phys. Rev. E **82**, 026201 (2010).
[28] F. J. Arranz, L. Seidel, C. G. Giralda, R. M. Benito, and F. Borondo, Phys. Rev. E **87**, 062901 (2013).
[29] M. Robnik and M. V. Berry, J. Phys. A **18**, 1361 (1985).
[30] J. U. Nöckel and A. D. Stone, Nature **385**, 45 (1997).